AN ADAPTIVE DENOISING METHOD USED IN MRI

Huaizhong Zhang, Xianghua Xie

Department of Computer Science, Swansea University, UK, SA2 8PP

ABSTRACT

This paper proposes an adaptive denoising method that can significantly reduce Rician noise in magnetic resonance imaging (MRI). We use a Rayleigh kernel in the denoising processing of self-snakes instead of the Gaussian kernel that is usually used. The Rayleigh kernel is adaptively constructed according to the estimated standard deviation of Rician noise in images. The numerical implementation is carried out by applying the level-set techniques with a semi-implicit scheme. Experimental results in both synthetic and real images demonstrate the effectiveness and advantages of the proposed method in comparison with the traditional methods.

Index Terms— MRI, denoising, self-snakes, Gaussian, Rayleigh

1. INTRODUCTION

In magnetic resonance imaging (MRI), the raw signal is acquired in a complex space which is corrupted by white Gaussian noise. For presenting signal, the complex data is transformed to a magnitude image and then the Rician-distributed noise is generated from both real and imaginary parts [1]. This Rician noise can significantly affect the quantitative analysis of MRI images, particular in the case of Diffusion-Weighted MRI (DW-MRI), where the nature of data acquisition is more susceptible to Rician noise because higher water anisotropy along tissues produces progressively lower intensities in images. Although noise can be reduced by averaging multiple acquisitions during acquisition processes, this is time-consuming and may not be a suitable alternative in clinics, particularly in high angular resolution DW-MRI where the number of acquired gradient directions can come to hundreds and may result in prohibitive scan durations. Thus, post-processing denoising techniques have been extensively employed in MRI and then a variety of methods have been proposed to restore the true underlying signal given a noisy image over the years.

Generally, most denoising methods are based on the signal averaging principle, which may be the stochastic methods based on statistical strategy or the deterministic methods based on variational formulation [2]. In this paper, we focus on discussing the application of a variational technique in MRI image denoising. Variational methods have been found effective in various applications, e.g. image segmentation [3, 4]. In principle, the variational techniques of image denoising are constructed in a continuous domain by applying a corresponding partial differential equation (PDE) solution scheme, which the seminal idea was from the anisotropic diffusion method proposed by Perona and Malik [5]. This denoising formulation can reduce noise at a faster rate and avoid the problems such as edge blurring in comparison to other schemes [2]. Thus, numerous PDE-based methods have been proposed by applying different theoretical ideas for dealing with various image modalities such as mean-curvature filtering, total variation and self-snakes [2, 5, 6]. In MRI, this denoising formulation has been used to perform anisotropic smoothing, diffusion profile restoration and DW-MRI image denoising [7, 8, 9]. However, such denoising formulation typically imposes certain models on local image structures that are often too simple to capture the complexity of anatomical MRI images [10]. In particular, a Gaussian smoothing kernel is usually employed in relevant solution schemes, which does not actually respect the nature of noise distribution in MRI images such as the Rician distribution. These methods could be reasonable only when signal-to-noise ratio (SNR) is greater than 3 where Rician noise is approximated as a Gaussian [1]. However, sometimes the SNR in MRI images is quite low because a considerable amount of noise is presented in acquisition processes. On the other hand, for enhancing and denoising in images, self-snakes [6], as a typical PDE-based method, was firstly induced from the mean curvature motion that the auxiliary level-set function is the image itself. It can effectively deal with the Gaussian noise by using a Gaussian smoothing kernel. But, self-snakes has not been applied to MRI images so far because the inherent Rician noise cannot be appropriately removed by a Gaussian kernel. In our method, we propose to use a Rayleigh kernel instead of a Gaussian one in the denoising process of self-snakes. Furthermore, by constructing a Rayleigh kernel in terms of the standard deviation σ of the estimated noise in images, the denoising process can be adaptive to images so as to improve its effectiveness. For demonstrating the performance, the proposed method is applied to both synthetic and real images. The traditional methods, self-snakes with the Gaussian kernel and the non-local method (NLM) [11], are employed to do the performance comparison.

In the following section, we introduce the proposed method, together with the presence of the numerical imple-

mentation; the experimental results are presented in Section 3; finally, the paper is concluded in Section 4.

2. METHOD

2.1. Self-snakes

Self-snakes [6] has been proposed for image denoising (or enhancement), which is a specific variant of mean curvature motion (MCM). It can be directly derived from the geodesic active contours (GAC) [2] by assuming the auxiliary level-sets function u to be the image I. The image evolution equation can then be described:

$$\frac{\partial I}{\partial t} = \|\nabla I\| div(g(\|\nabla I_\sigma\|)\frac{\nabla I}{\|\nabla I\|}), \quad (1)$$

where g is a positive decreasing function (stopping function) and I_σ is a smoothing version of the image by convolving a Gaussian kernel.

2.2. Denoising principle and Rayleigh smoothing kernel

The inherent denoising idea behind eq. (1) is to carry out a Gaussian filtering in a nonlinear way, removing the noise while allowing the preservation of significant image features, such as boundaries and corners [2]. This denoising technique has two aspects of the methodology:

- Smoothing strategy: inside the regions where the gradient magnitude is weak, so eq. (1) acts like the heat equation, resulting in the simple isotropic smoothing (a Gaussian convolution).

- Preserving strategy: near the region's boundaries where the gradient magnitude is large, the motion of the image level-set is 'stopped' and the edges are preserved.

In eq. (1), $I_\sigma = G_\sigma * I$, it is the Gaussian convolution and performs local averaging, where the standard deviation σ indicates the level at which averaging is being carried out. Therefore, I_σ is the smoothing output at the level σ and it can be intuitively interpreted that features of size smaller than $O(\sigma)$ have been smoothed significantly as noise and only those features of size larger than $O(\sigma)$ are still readable in I_σ. Furthermore, in the frequency domain, a two-dimensional Gaussian kernel can be shown in Fig. 1(b) and it is a low-pass filter that inhibits high frequencies. The denoising process is to smooth a pixel with a weighted average of the neighbour pixels by convolving with the Gaussian kernel. However, this smoothing is isotropic; it is not associated with the nature of image noise, and the performance is the same in all directions [2]. For Rician noise in MRI, such as shown in Fig. 1(a), the noise is inhomogeneous and the Gaussian smoothing will not be effective as that in the case of the Gaussian noise. Thus, an anisotropic smoothing strategy will be desirable.

Due to image quality greatly depending on acquisition processes in MRI, we assume that the noise level for a given

sequence should be constant on the same scanner in this study, which is similar to the assumption in [12]. Thus, we use the noisy regions extracted from the background of MR images for estimating an average level of noise over all images. In addition, because Rician is a Rayleigh distribution in background where the signal is usually considered as zero, we use a Rayleigh distribution in background as the estimate of noise distribution in images,

$$R_\sigma(x) = \frac{x}{\sigma^2} exp\{-\frac{x^2}{2\sigma^2}\}, x > 0, \quad (2)$$

where the standard deviation σ is estimated by the method introduced in [13]. Fig. 1(a) is the background in a real image and its histogram is shown in Fig. 1(d) as a typical Rayleigh distribution ($\sigma = 34$). Considering the anisotropic property of Rician noise in MRI images, an anisotropic kernel can perform better than an isotropic one by inhomogenously smoothing the surrounding artefacts. Hence, we use the Rayleigh distribution (eq. (2)) to construct an anisotropic smoothing kernel for smoothing the image in eq. (1) instead of the Gaussian kernel. Eq. (1) can be expressed as follows:

$$\frac{\partial I}{\partial t} = \|\nabla I\| div(g(\|\nabla I_{R_\sigma}\|)\frac{\nabla I}{\|\nabla I\|}), \quad (3)$$

where I_{R_σ} is to smooth the image by convolving with a Rayleigh kernel with the standard deviation σ.

The anisotropic action of the Rayleigh kernel in eq. (3) can be interpreted in the frequent domain. Let $F[I](\omega)$ denote the Fourier transform of image intensity I. The Fourier transform of the convolution by a Rayleigh with I can be derived as follows:

$$F[R_\sigma](\omega) = \sqrt{1 + \frac{\pi}{2}\sigma^2\omega^2} exp\{-\frac{\sigma^2\omega^2}{2}\} exp\{i\phi\} F[I](\omega) \quad (4)$$

where $\phi = arctan(-\sqrt{\frac{\pi}{2}}\sigma\omega)$. This result (eq. (4)) of the Fourier transform indicates the frequency response of a Raleigh convolution filter, i.e. its effect on different spatial frequencies. Fig. 1(e) illustrates the frequency response of a Rayleigh filter (magnitude $\sqrt{1 + \frac{\pi}{2}\sigma^2\omega^2} exp(-\frac{\sigma^2\omega^2}{2})$) with $\sigma = 34$. The spatial frequency axis is marked in cycles per pixel and it shows that no value above 0.4 has a real meaning. This demonstrates that the convolution is a low-pass filter and the anisotropic action will be performed along the phase ϕ.

In general, the smoothing idea is to use this Rayleigh distribution as a 'point-spread' function and this can be achieved by convolution with a Rayleigh kernel. In practice, we need to provide a discrete approximation to the Rayleigh function for performing the convolution since the image is described as a collection of discrete pixels. Due to its distribution being concentrated around the maximal point $x = \sigma$, the Rayleigh distribution is effectively approximate to zero when beyond the interval $[\sigma/4, 2\sigma]$. We illustrate an example of Rayleigh kernel ($\sigma = 34$) in Fig. 1(c), which shows anisotropic property rather than a Gaussian kernel's isotropy in Fig. 1(b). In
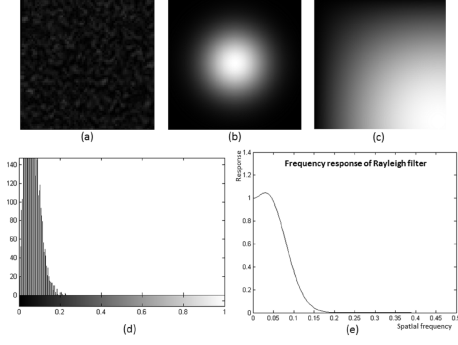
Fig. 1. Riacian noise in a real MR image (a) and its intensity distribution (d); the Gaussian kernel (b) and the Rayleigh's kernel (c); (e) shows frequency response of Rayleigh filter ($\sigma = 34$).

the following, we call this self-snakes using the Rayleigh kernel as the Rician self-snakes and that is with the Gaussian kernel as the Gaussian self-snakes.

2.3. Semi-implicit scheme and numerical implementation

For numerical implementation, a semi-implicit scheme [10] is employed, which is much faster and more efficient than the traditional explicit scheme. In our numerical implementation of the iterative approximation, the primary steps include discretizing the diffusion equation eq. (2), forming a semi-implicit linear system and developing an iterative approximation scheme. Eq. (2) is then discretized as given in the following formula:

$$I^{n+1} = \frac{1}{2} \sum_{l \in \{x,y\}} (I - 2\tau A_l(I^n))^{-1} I^n \tag{5}$$

where $A_l(u^n) = (\hat{a}_{ijl}(u^n))$ is the intermediate numerical matrix in the iterative process that can be expressed in detail as follows.

$$\hat{a}_{ijl}(u^n) = \begin{cases} a_i \|\nabla u\|_i^n \dfrac{2}{\left(\frac{\|\nabla u\|}{g}\right)_i^n + \left(\frac{\|\nabla u\|}{g}\right)_j^n}, & j \in \mathcal{N}_l(i), \\ -a_i \|\nabla u\|_i^n \sum\limits_{m \in \mathcal{N}_l(i)} \dfrac{2}{\left(\frac{\|\nabla u\|}{g}\right)_i^n + \left(\frac{\|\nabla u\|}{g}\right)_m^n}, & j = i, \\ 0, & others, \end{cases} \tag{6}$$

where $N_l(i)$ is the neighbor point in $l \in \{x, y\}$ direction.

3. EXPERIMENTAL RESULTS

For validating the performance, we apply the proposed method to both synthetic data and real data with various Rician noise levels. The quality of image restoration was assessed in terms of SNR according to actual situation. The SNR is estimated as the mean signal in the image divided by the σ of the background noise. The σ value is estimated based on measuring the proximity of the Rician toward Rayleigh or the Gaussian. For accurately assessing image quality, we estimate SNRs on the background and foreground of an image separately similar to the methods in [12, 14]. In our scheme the four rectangular regions in background are selected for averaging the calculations and the maximised rectangular

region in foreground is selected according to actual images. The standard deviation used in the kernels is named SD in the following.

3.1. Results on synthetic data

We chose an image (Fig. 2(a)) and corrupted it with the Rician noise of $\sigma = 50$ (Fig. 2(b)). For examining the SD sensitivity in the Rayleigh kernel, we applied the proposed method with various kernel SD values in Fig. 2(b) (30 iterations). Fig. 2(c) shows that the performance will be best at $SD = 3\sigma = 150$ by considering the SNRs in both background and foreground. However, Fig. 2(f) present a over-smoothing image using $SD = 3\sigma$. Similarly, the edge is slightly blurred in Fig. 2(e), which the SD is 2σ. Fig. 2(d) shows that the edge can preserve well although the SNR is not as good as that in Fig. 2(e-f). Thus, for balancing the smoothing effect and actual performance of the proposed method, we will use $SD = \sigma$ in the experiments.
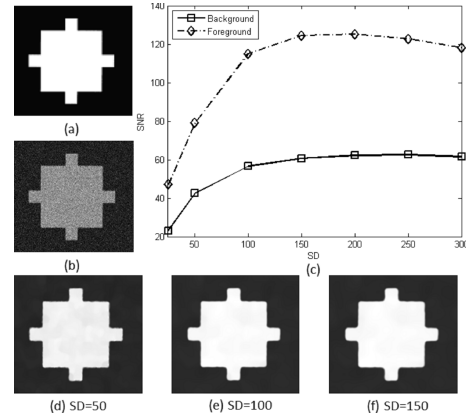

Fig. 2. (a) the original image, (b) the corrupted image with the noise of $\sigma = 50$, (c) the SNR results of performing our method with various SD values in the background and foreground of (b), (d-f) are the results using different SD values.

For further validating the proposed method, we generated a series of noisy images from the noise-free image, Fig. 2(a), with different σ (10, 20, 30, 40, 50, 60, 70, 80) of Rician noise. Our method, NLM and the Gaussian self-snakes have been applied to perform the denoising processes on these images. For the sake of consistency and fairness, the same number of iterations (30) and the SD value ($=\sigma$) in the relevant kernels have been used in the denoised methods. Fig. 3(a-b) illustrates that the Rician self-snakes performs significantly better than the other two methods in both background and foreground of all the cases except the case of SD=10. The performance of our method is very similar to that of the Gaussian self-snakes in the case of SD=10 because the Rician is approximated to a Gaussian when SNR is high. Fig. 3(c-e) show the resulting images using the relevant methods in Fig. 2(b) respectively.

3.2. Results on real data

For examining the effectiveness of the proposed method in real MRI images, a sequence of slices 51-60 (from a DTI
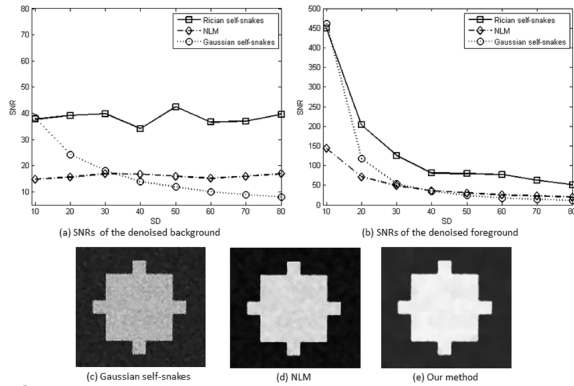
Fig. 3. (a) and (b) are the SNRs of the resulting images using the methods in the synthetic images with different noise levels. (c-e) show the resulting images by applying the methods in Fig. 2(b).

volume of 30 orientations with the magnetic gradient = $1500 s/mm^2$) in DW-MRI are used to perform the denoising process by applying the proposed method, NLM and the Gaussian self-snakes. Due to the estimated $\sigma = 34$ in the slices, the $SD = 34$ is used in the methods as discussed above. The number of iterations is 60 for all denoising processes. In Fig. 4(a-b), the SNRs of the denoised images are illustrated according to the results using the methods in each slice. Fig. 4(a) presents the SNRs in background and Fig. 4(b) for foreground. The results show that the performance of the Gaussian self-snakes is slightly better than that of NLM in these real images. We can see that the proposed method performs significantly better than the other two methods in both the background and foreground. Fig. 4(c) shows Slice 51 and The resulting images for Slice 51 are presented in Fig. 4(d-f).
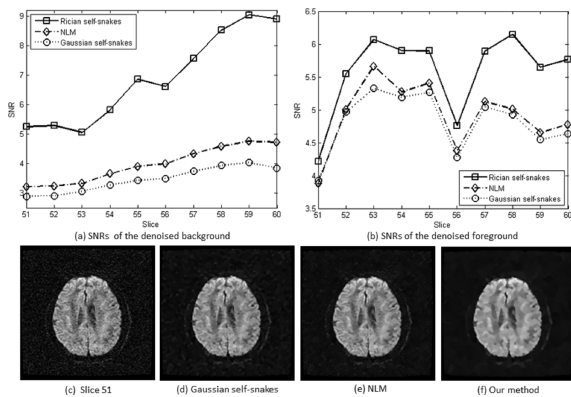
Fig. 4. The SNRs of the resulting images using various methods in Slices 51-60 and an resulting example for Slice 51. (a) the SNRS of the background, (b) the SNRs of the foreground, (c) is Slice 51 and (d-f) show the resulting images by applying the methods in Slice 51.

4. CONCLUSION

In this paper we have described a novel use of self-snakes in MRI. For adaptive to actual noise situation in MRI, we proposed to use a Rayleigh kernel instead of the traditional Gaus-

sian kernel for removing Rician noise efficiently. In addition, the Rayleigh kernel is adaptive to be designed according to the standard deviation levels in noisy images. The numerical approximation is implemented by applying the semi-implicit solution scheme in the level-set framework. Experimental results for both synthetic and real data demonstrate that the proposed method can deal with Rician noise effectively in comparison with the traditional methods such as the Gaussian self-snakes and NLM.

5. REFERENCES

[1] H. Gudbjartsson and S. Patz, "The rician distribution of noisy mri data," *Magn Reson Med.*, vol. 34, pp. 910–914, June 1995.

[2] G. Aubert and P. Kornprobst, *Mathematical problems in image processing*, Springer, 2006.

[3] X. Xie and M. Mirmehdi, "Level-set based geometric colour snake with region support," in *IEEE ICIP*, 2003, vol. 2, pp. 153–156.

[4] X. Xie and M. Mirmehdi, "Colour image segmentation using texems," *Annals of the BMVA*, vol. 1, no. 6, pp. 1–10, 2007.

[5] P. Perona and J. Malik, "Scale-space and edge detection using anisotropic diffusion," *IEEE Trans. PAMI.*, vol. 12, pp. 629–639, Dec. 1990.

[6] G. Sapiro, "Vector (self) snakes: a geometric framework for color, texture, and multiscale image segmentation," in *IEEE ICIP*, 1996, vol. I, pp. 817–820.

[7] D. Tschumperle and R. Deriche, "Anisotropic diffusion partial differential equations in multi-channel image processing : Framework and applications," in *Advances in Imaging and Electron Physics*, 2007, vol. I.

[8] T. McGraw, B. Vemuri, E. Ozarslan, Y. Chen, and T. Mareci, "Variational denoising of diffusion-weighted mri," *Inverse problem and imaging*, vol. 3, pp. 625–48, March 2009.

[9] Y. Kim, P. Thompson, and L. Vese, "Hardi data denoising using vectorial tv and logarithmic barrier," *Inverse Problems and Imaging*, vol. 4, pp. 273–310, April 2010.

[10] S. Awate and R Whitaker, "Feature-preserving mri denoising: a nonparameteric empirical bayes approach," *IEEE Trans. On Medical Imaging*, vol. 26, pp. 1242–55, September 2007.

[11] A. Buades, B. Coll, and J. Morel, "A review of image denoising algorithms , with a new one," *Multscale Model., SIMUL.*, vol. 4, pp. 490–530, February 2005.

[12] P. Coupe, J. Manjon, E. Gedamu, D. Arnold, M. Robles, and D. Collins, "Robust rician noise estimation for mr images," *Medical Image Analysis*, vol. 14, pp. 483–93, April 2010.

[13] J. Rajan, D. Poot, J. Juntu, and J. Sijbers, "Noise measurement from magnitude mri using local estimates of variance and skewness," *Physics in Medicine and Biology*, vol. 55, pp. 441–49, 2010.

[14] S. Aja-Fernandez, C. Alberola-Lopez, and C. Westin, "Noise and signal estimation in magnitude mri and rician distributed images: a lmmse approach," *IEEE Trans. Image Processing*, vol. 17, pp. 1383–98, August 2008.